AIP | Journal of Applied Physics

355, 532, and 1064nm picosecond laser interaction with grass tissues

Jaehun Kim and Hyungson Ki

Citation: J. Appl. Phys. **112**, 114908 (2012); doi: 10.1063/1.4768684
View online: http://dx.doi.org/10.1063/1.4768684
View Table of Contents: http://jap.aip.org/resource/1/JAPIAU/v112/i11
Published by the AIP Publishing LLC.

JOURNAL OF APPLIED PHYSICS **112**, 114908 (2012)

355, 532, and 1064 nm picosecond laser interaction with grass tissues

Jaehun Kim and Hyungson Ki[a)]
School of Mechanical and Advanced Materials Engineering, Ulsan National Institute of Science and Technology (UNIST), Ulsan, South Korea

(Received 20 September 2012; accepted 6 November 2012; published online 10 December 2012)

In this article, we investigate how 355, 532, and 1064 nm picosecond lasers interact with grass tissues. We have identified five interaction regimes, and based on this classification, interaction maps have been constructed from a systematic experiment. The optical properties of light absorbing grass constituents are studied theoretically in order to understand how and how much light is absorbed by grass tissues. Scanning electron microscopy and optical microscopy are employed for observing morphological and structural changes of grass tissues. To the best of the authors' knowledge, this is the first investigation into laser interaction with plant leaves and reveals some fundamental findings regarding how a laser interacts with grass tissues and how plant leaves can be processed using lasers.
 [http://dx.doi.org/10.1063/1.4768684]

I. INTRODUCTION

Pulsed lasers, especially short pulse lasers, have been proved to be an efficient way to process not only common engineering materials but also hard-to-process biomaterials, such as heart tissue, teeth, and cornea.[1] Even some researchers studied laser interaction with cellulose, gelatin and papers[2–4] for possible practical applications. In spite of its huge potential importance in many disciplines, however, laser interaction with plant leaves have not been studied to date.

It is well known that laser material interaction exhibits diverse and complex physical phenomena depending on the target material and environment.[5–10] Plant leaves, especially green leaves, are common landscaping and agricultural materials and lasers could be creatively used for many possible innovative applications. Plant leaves exhibit very complicated optical properties because they have complex multilayer structures and are basically a composite of many dissimilar optical elements, including photosynthesizing pigments. Photosynthesis is the process of synthesizing glucose ($C_6H_{12}O_6$) from water and carbon dioxide using the energy of sunlight. As well known, chlorophylls can absorb the visible light well, especially blue and red lights, and that is why most plant leaves are green.[11] Carotenoids, which are yellow or orange pigments, have a different absorption spectrum from chlorophylls. Water is the largest constituent of plant leaves and has an interesting light absorption characteristic. Therefore, in order to study how a laser beam interacts with plant leaves, the light absorption characteristics of all major optical elements in plant leaves must be clearly understood.

This study investigates how a laser interacts with grass tissues using a 355, 532, and 1064 nm picosecond laser. Grass is selected because it is the most commonly used landscaping plant and can be prepared for experiment with ease. In addition, grass is a monocotyledon and has a relatively simple leaf mesophyll structure. Out of many grass types, Kentucky bluegrass (*Poa pratensis*), which is one of the top three pasture grasses in the United States,[12] is used. We have first identified the dominant light-absorbing grass constituents as a function of light wavelength from a theoretical study of grass optical properties. A systematic experiment is also conducted to construct an interaction map for laser grass-tissue interaction over a wide range of process parameters, which shows how a particular process regime changes on the interaction map as the laser wavelength changes from 355 to 532 to 1064 nm. Scanning electron microscopy (SEM) and optical microscopy are employed for studying morphological and structural changes in grass tissues after laser irradiation. To the best of the authors' knowledge, this work is the first investigation into laser interaction with plant leaves and reveals some fundamental findings regarding how a laser interacts with grass tissues and how plant leaves can be processed using lasers.

II. THEORETICAL INVESTIGATION OF GRASS OPTICAL PROPERTIES

In order to study the underlying mechanisms for laser-tissue interaction, we need to first investigate how laser energy is absorbed by grass tissues. There are largely three kinds of light absorbing agents in grass: water, pigments and dry matter.[13] Water is apparently the largest constituent of plant leaves and its optical properties are well documented in the literature.[14] In typical plant leaves, two types of pigments exist: chlorophylls and carotenoids.[15] Although two kinds of chlorophylls (chlorophyll a and chlorophyll b) and numerous kinds of carotenoids (e.g., β-carotene, lutein, violaxanthin, and neoxanthin) exist in most plant leaves and their relative concentrations vary from one plant to another, we will just categorize leaf pigments as chlorophylls and carotenoids in this study. The rest of the leaf consists of cellulose, hemicellulose, proteins, lignins, and startch, but they will be lumped together and called as dry matter in this study.[15] In other words, dry matter refers to leaf material removed of water.

The energy transfer mechanism inside grass blades can be studied using the Beer-Lambert law. In this law, the

[a)]Author to whom correspondence should be addressed. Electronic mail: hski@unist.ac.kr.

intensity of light (I) inside a medium decreases exponentially, where the exponent is proportional to both the absorption coefficient (α) and the propagation distance (z):

$$I = I_0 \exp(-\alpha z). \quad (1)$$

Therefore, if α values for all major optical elements of grass tissues (i.e., pigments, water, and dry matter) are determined, we can predict how and how much laser energy is transferred to grass tissues. For water, the absorption coefficient versus wavelength is well studied and we adopted the result by Hale *et al.*[14] Unlike water, however, pigments must be extracted from leaves in a liquid to measure their optical properties. Therefore, their actual absorption coefficients are given as functions of their concentrations (C), and in plant biochemistry the specific absorption coefficient (a) is normally used, which is absorption coefficient per concentration and has units of cm^2/mg. Owing to this difference, we converted the absorption coefficient data of water to the specific absorption coefficient by dividing it by the density of water ($\rho_w = 1\ g/cm^3$).

The optical properties of plant leaves considering leaf mesophyll structures have been studied mainly for remote sensing applications.[13,16,17] In this study, specific absorption coefficients of chlorophylls (a_{chl}), carotenoids (a_{car}), and dry matter (a_{dm}) are obtained from Ref. 15 and are shown in Figure 1 together with the specific absorption coefficient of water (a_w).

As shown in Figure 1, chlorophylls and carotenoids show a strong absorption characteristic up to around 700 nm and 500 nm, respectively. As expected, chlorophylls absorb blue and red colors well, and carotenoids absorb yellow to orange colors well. On the other hand, dry matter, which is obtained by removing water from leaves, has about 5 orders of magnitude lower absorption coefficient values than pigments and decreases slowly as the light wavelength increases. In this wavelength range, water is the least significant light absorbing component, even worse than dry matter, and it has the minimum absorption at around 475 nm. For comparison purposes, the specific absorption coefficients of

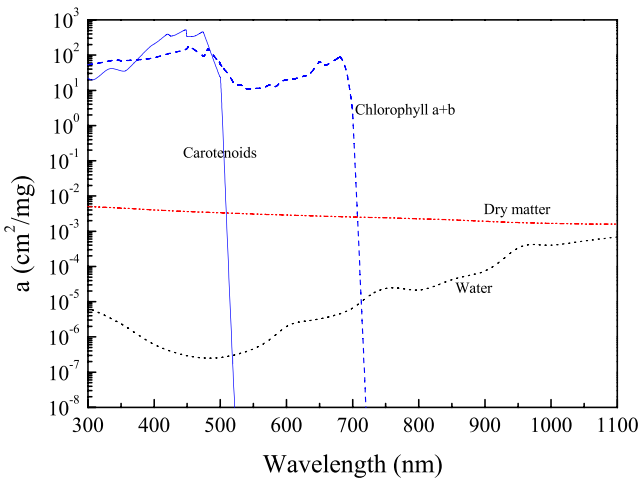

FIG. 1. Specific absorption coefficients of water, chlorophylls, carotenoids, and dry mater. (Reconstructed using data from Refs. 14 and 15).

grass constituents at the three wavelengths are summarized in Table I.

To understand the relative importance of each grass constituent in absorbing light energy, we need to determine their concentrations in a typical grass blade. In the study of thin structures such as plant leaves, normally concentration and density are calculated per unit surface area. Dong *et al.* reported that the leaf area density (mass per unit area of leaf, σ_{grass}) of fresh Kentucky bluegrass leaves is $5.76\ mg/cm^2$ (the reciprocal of the specific leaf area, 173.5 cm^2/g).[18] Applying the average water content (or mass fraction f_w) of plant leaves, 66.4%, reported in Ref. 17 to grass, the water concentration in grass (per unit area) is calculated as

$$C_w = f_w \sigma_{grass} = 3.82\ mg/cm^2. \quad (2)$$

The chlorophylls and carotenoids mass fractions (f_{chl} and f_{car}) for fresh Kentucky bluegrass are reported as 6.83 mg/g and 0.795 mg/g, respectively.[19] Using these values, pigment concentrations can be easily calculated by multiplying leaf area density as:

$$C_{chl} = f_{chl} \sigma_{grass} = 0.0393\ mg/cm^2, \quad (3)$$

$$C_{car} = f_{car} \sigma_{grass} = 0.00458\ mg/cm^2. \quad (4)$$

And, the concentration of dry matter can be estimated as,

$$C_{dm} \simeq \sigma_{grass} - C_w = 1.94\ mg/cm^2. \quad (5)$$

The concentrations of major components are summarized in Table II.

Now that specific absorption coefficients and concentration values are all determined, the actual light absorption characteristics can be calculated by multiplying the two together ($a \times C$), as shown in Figure 2. Note that, because C is concentration per unit grass surface area, $a \times C$ represents the absorption characteristic of grass with grass thickness accounted for.

Using Figure 2, we can determine which component is a dominant player in the absorption of light at a given laser wavelength. Note that because concentration per unit surface area of grass is multiplied in obtaining Figure 2, this figure shows the absorption characteristics of the four constituents especially for grass. The green solid line shows the $a \times C$ value for all pigments combined (i.e., chlorophylls and carotenoids). It is shown that from 300 nm to ~700 nm, pigments are the predominant light absorbing element and the absorption by dry matter and water is virtually negligible. Also, as clearly seen, chlorophylls are dominant over carotenoids. On the other hand, from ~700 nm to 1100 nm the situation becomes totally different and light absorption occurs due to

TABLE I. Specific absorption coefficients of water, chlorophyll, carotenoids, and dry matter.

λ (nm)	a_w (cm^2/mg)	a_{chl} (cm^2/mg)	a_{car} (cm^2/mg)	a_{dm} (cm^2/mg)
355	0.0000021	69	35	0.0045
532	0.00000035	15.1	0	0.0031
1064	0.00061	0	0	0.0016

TABLE II. Concentrations of water, chlorophylls, carotenoids, and dry matter in a typical Kentucky bluegrass blade (expressed as mass contained in unit area of grass blade).

C_w (mg/cm^2)	C_{chl} (mg/cm^2)	C_{car} (mg/cm^2)	C_{dm} (mg/cm^2)
3.82	0.0393	0.00458	1.94

dry matter and water. Also, the strength of absorption is 2∼3 orders of magnitude smaller. In this wavelength range, dry matter is dominant over water in absorption performance, but as the wavelength increases the gap in between decreases and at around 1100 nm dry matter absorbs slightly more light than water. Table III summarizes $a \times C$ values for 355, 532, 1064 nm wavelengths. The overall absorption characteristic of grass tissues can be explained by the sum of all the $a \times C$ values ($\sum_i a_i C_i$), which are also listed in Table III.

One more thing to consider is the effective optical penetration depth (δ) for each wavelength. The effective optical penetration depth δ equals the reciprocal of the effective absorption coefficient of grass and can be estimated by dividing the average grass thickness by $\sum_i a_i C_i$ as follows:

$$\delta = \frac{1}{\alpha_{grass}} \approx \frac{\ell_{grass}}{\sum_i a_i C_i}, \tag{6}$$

where ℓ_{grass} is the average thickness of grass blades (110 μm). Note that as shown in Table III, for 355 nm wavelength the penetration depth is roughly 1/3 of the thickness of the grass and we believe the laser energy heats up the grass very effectively. For 532 and 1064 nm, the corresponding penetration depths are 183 μm and 20370 μm, respectively, so we can learn that light absorption is extremely small for $\lambda = 1064$ nm.

III. CLASSFICATION OF INTERACTION REGIMES

To investigate how laser interacts with grass tissues experimentally, a picosecond laser (Coherent Talisker 355–4), which generates 355, 532, and 1064 nm wavelengths,

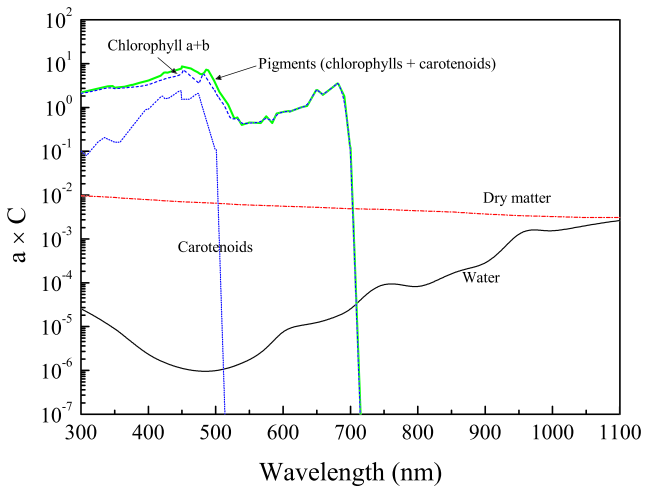

FIG. 2. Spectral absorption characteristics ($a \times C$) of major constituents of Kentucky bluegrass considering the thickness of the grass blade.

TABLE III. axC for water, chlorophylls, carotenoids, and dry matter, and the effective penetration depth.

λ (nm)	$a_w C_w$	$a_{chl} C_{chl}$	$a_{car} C_{car}$	$a_{dm} C_{dm}$	$\sum_i a_i C_i$	δ (μm)
355	0.0000080	2.71	0.160	0.0087	2.88	38
532	0.0000013	0.593	0	0.0060	0.60	183
1064	0.0023	0	0	0.0031	0.0054	20370

was used in this study. The laser beam is linearly polarized with a pulse width of 10 ∼ 15 ps and a pulse repetition rate of 200 kHz. As a target, Kentucky bluegrass with an average blade thickness of 110±5 μm is selected. Because the central stem of a grass blade is much thicker, we measured the grass thickness away from that part. One problem experienced in dealing with grass is that it is very difficult to have a laser beam focused on its surface because it is flexible. To resolve this issue, we made a jig out of PMMA and fixed the grass blades as shown in Figure 3. For all three wavelengths, the same beam size of 21 μm is used to avoid the beam size effect.

One of the primary objectives of this study is to investigate laser grass-tissue interaction over a wide range of primary interaction parameters (i.e., laser intensity and scanning speed), so that interaction maps can be constructed. Since the size of the map is inherently set by the limitations of equipment, we designed the experiment based on the minimum and maximum values attainable (see Table IV). The experiments were conducted from December 2011 to January 2012, which is a winter season in Korea.

As shown in Figure 4, after analyzing the optical micrographs of processed grass blades, we classified the interaction regimes into five: no visual change, decoloration, partial cut, through cut and carbonization in the order of increasing energy absorption. Up to a certain threshold energy value, the absorbed laser energy does not cosmetically affect the grass blade and there is no noticeable visual change at the surface of the grass (Figure 4(b)). Note that in the case of green plant leaves, the pigments can absorb light up to around 700 nm if the light energy is not much higher than the demand of metabolites. If the light energy is large, however, it is reported that to avoid damage chloroplasts move from the cell surface to the side walls of the cells and/or the excess energy is dissipated as heat.[11] As long as the amount of heat generation is below the tissue damage threshold, the energy is nondestructively dissipated inside the grass blade and there will be no visual change in grass tissues.

If the light energy is larger than the thermal capacity of the plant tissues, now the grass tissues will be thermally damaged. This is evidenced by Figure 4(c), where decoloration occurs and the grass surface becomes whitened. This change in color means that the reflection pattern in the visible range is modified, and we believe that this is caused by the damaged chlorophylls and/or carotenoids. Note that as seen in Figure 2 light absorption (and therefore reflection) is dictated by pigments in the visible spectrum.

One more thing to consider at this point is that once laser energy is larger than what pigments can handle, we believe that pigments are no longer able to absorb light as pigments

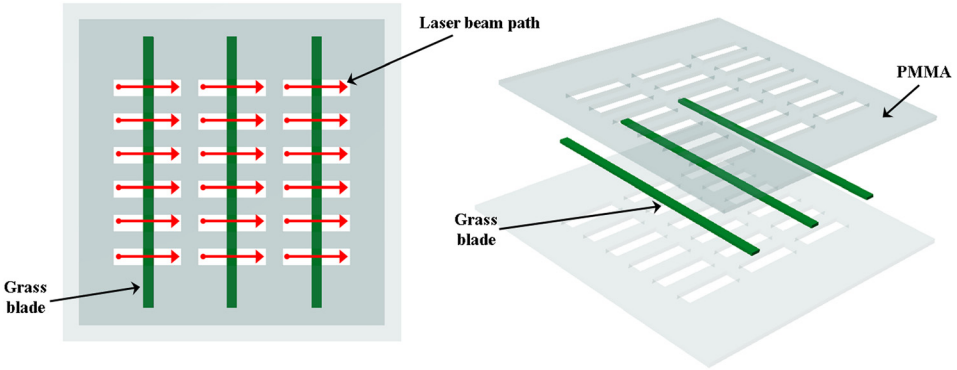

FIG. 3. Schematic view of the jig used for fixing grass blades. The red line shows the laser beam scanning direction and the green lines are grass blades.

and further light absorption occurs via other grass constituents, such as dry matter and water. Therefore, the actual specific absorption coefficient could be lower than shown in Figure 2.

As the laser energy level becomes even higher, now the ablation effect is more visually noticeable and cutting starts to occur. As shown in Figures 4(d) and 4(e), the quality of the cut is very good and there is no sign of damage other than the cut made. Here, we defined partial-cut and through-cut depending on whether or not the grass blade is fully separated. The mechanism of this cutting process will be discussed with SEM images of cross-sections in the next paragraph. Finally, when the laser energy is much larger than the amount required for clean through-cut, the grass blade is cut with signs of carbonization around the cut area (Figure 4(f)). Carbonization is known to occur when the tissue temperature is above approximately 100 °C.[1] At this temperature, carbon is released and the tissue becomes blackened in color. One thing to note about carbonization is that it is a process in the thermal regime.[1] In other words, although a picosecond laser was used in this study, the interaction has a thermal nature.

Figures 5–7 present optical microscope images of grass blades and the corresponding SEM cross-section images for 355, 532, 1064 nm, respectively. In each figure, top rows correspond to carbonization, middle rows to onset of carbonization, and bottom rows to through-cut. The first thing to note is that there are hardly any differences between the three wavelength results. In other words, the morphologies of the cross-sections are virtually same. We believe that this is because light energy is transferred to tissues primarily via either pigments or dry matter. (Although water plays a role in the light absorption at 1064 nm, its contribution is smaller than that of dry matter.) Pigments and dry matter are basically part of grass tissues, but while water is also contained inside, it is fundamentally different from inherent grass tissues. In other words, in the former case, the energy is transferred first to tissues and then to water, but in the latter the order is opposite.

TABLE IV. Ranges of experimental parameters (laser power and scanning speed) for 355, 532, and 1064 nm wavelengths.

Wavelength (nm)	Power (W)	Scanning speed (mm/s)
355	0.01∼5	1∼500
532	0.01∼6.25	1∼500
1064	0.01∼13.8	1∼500

In all three wavelength cases, grass tissues become more damaged as the interaction regime changes from through-cut to carbonization. When a through-cut is made without carbonization, it looks like there is virtually no damage and water comes out from internal water channels. The original tissue morphology seems to be preserved well. In fact, these water droplets could be a proof that the absorption of light is not primarily by water: if light was absorbed primarily by water, most of water would evaporate and the chances of finding water near the cut area would be lower.

On the other hand, when full carbonization occurs (top rows in Figures 5–7), the cross-sections of the cuts are severely transformed, and it is almost impossible to find original tissue patterns. For all carbonization cases, regardless of the laser wavelength, water droplets are not observed, which means that water channels are damaged and closed.

IV. LASER GRASS-TISSUE INTERACTION MAP

In order to understand how a particular interaction regime changes as process parameters are varied, we conducted a systematic experiment over a wide range of process parameters and constructed interaction maps for 355, 532, and 1064 nm wavelengths. Primary process parameters are apparently peak laser intensity (I) and beam scanning speed (V_{scan}), and their ranges for the three wavelengths are listed in Table IV. We discretized these ranges using eight equally spaced points on a logarithmic scale, so that a total of 64 experiments were conducted to construct one map. Also, to improve the reliability, experiments were repeated twice for each wavelength. Note that experiments dealing with grass blades are very difficult and some variation between repeated experiments is inevitable, as evidenced in Figure 8.

In constructing interaction maps, we used *interaction time* (t_i) and *laser energy per unit laser scan length* (E') instead of the scanning velocity in order to obtain more physical insight. (Therefore, we generated two types of interaction maps.) Here, we defined the interaction time as

$$t_i = \phi \frac{D}{V_{scan}}, \tag{7}$$

where D is the focused beam diameter and ϕ is the duty cycle of the laser. The interaction time is roughly the duration of time a point on a grass blade interacts with the laser beam. Note that because a pulsed (picosecond) laser was

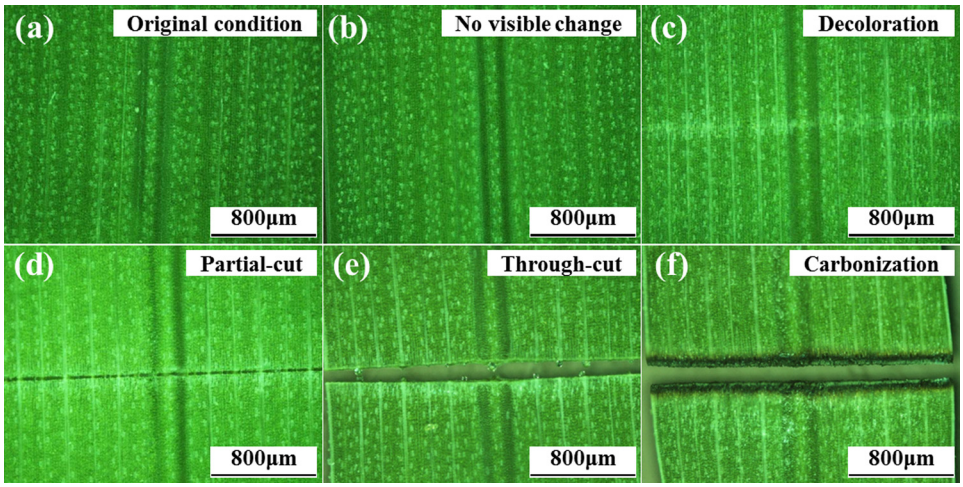

FIG. 4. Classification of laser-grass tissue interaction regimes.

used and the pulse width cannot be varied, this is the only time dimension associated with this problem. Energy per unit length in the beam scanning direction is calculated as the average laser power (P_{ave}) divided by the scanning velocity as shown follows:

$$E' = \frac{P_{ave}\Delta t}{\Delta \ell} = \frac{P_{ave}}{V_{scan}}. \tag{8}$$

Figure 8 presents interaction maps constructed for 355, 532, and 1064 nm lasers. In the left figures, interaction time is used as the x-axis, and the energy per unit scan length is used as the x-axis in the right figures. In both cases, y-axis represents the peak laser intensity in W/cm^2. In each figure, the state of the grass at the given experimental condition is expressed as one of the five colors following the classification defined in Figure 4. Because experiments were repeated twice, the first set of results is shown as circles and the second set shown as triangles, so that we can see the two results in one diagram. Note that if the slope is -1 on the $I - t_i$ diagram (left figures), it will appear vertical on the $I - E'$ diagram (right figures) because the intensity multiplied by the interaction time is the energy density. Also, a horizontal line on the $I - t_i$ diagram will appear also horizontal on the $I - E'$ diagram.

As clearly shown in Figure 8, as expected, overall as the intensity increases the interaction regime changes from no visible change to decoloration to partial-cut to through-cut to carbonization.

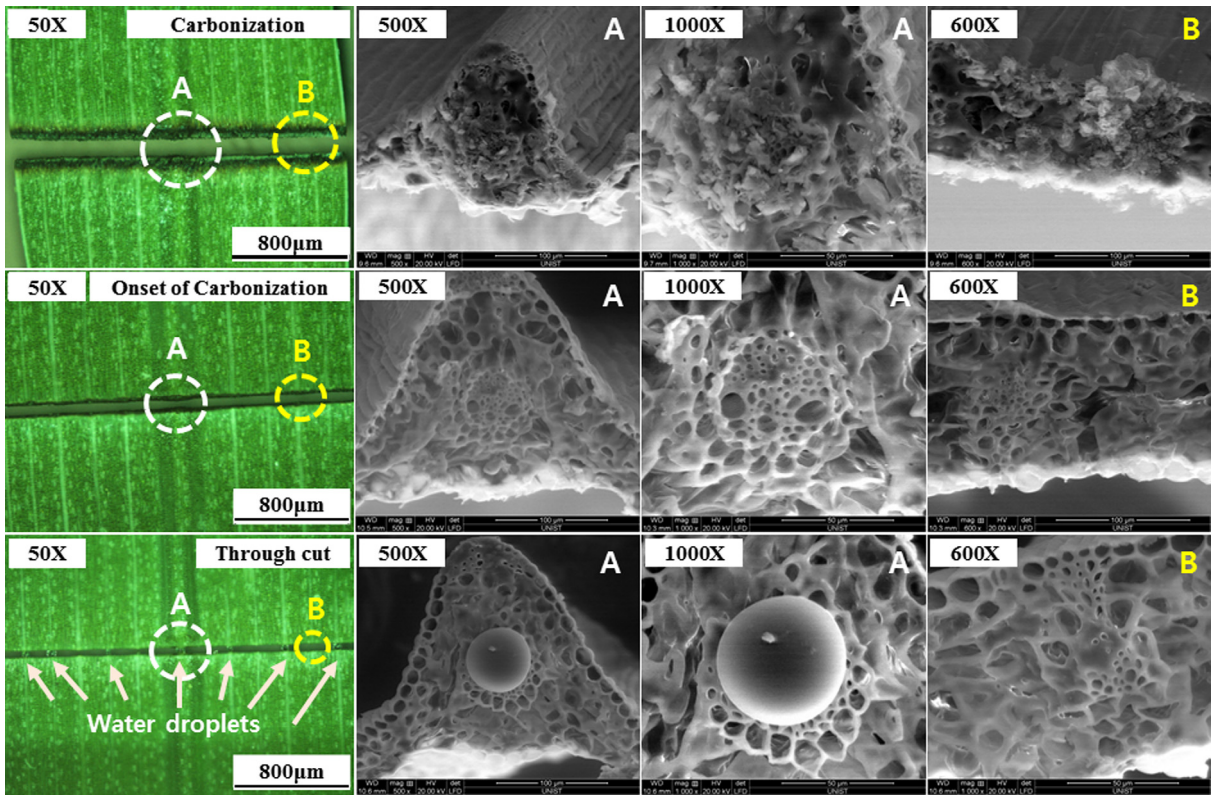

FIG. 5. Optical microscope and SEM images for 355 nm (Top row: 5 W and 1 mm/s, middle row: 2.058 W and 2.4 mm/s, bottom row: 0.349 W and 5.9 mm/s).

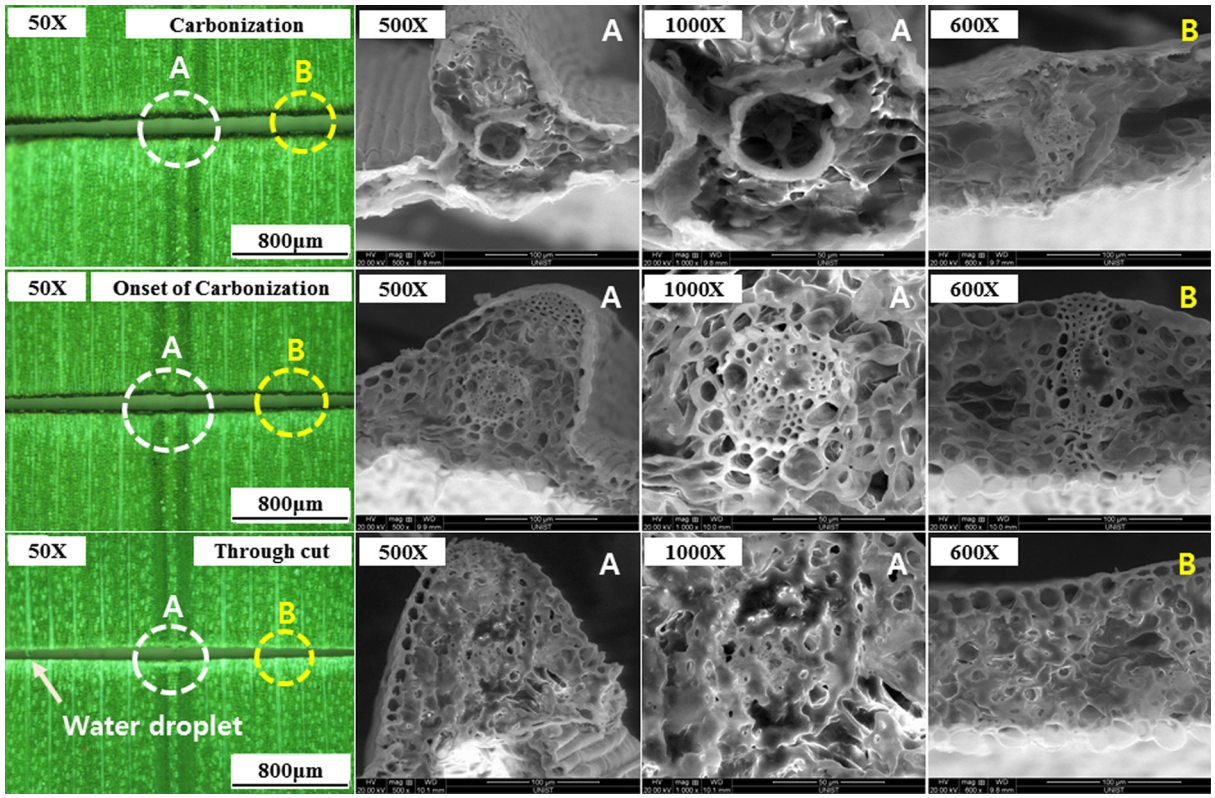

FIG. 6. Optical microscope and SEM images for 532 nm (Top row: 6 W and 1 mm/s, middle row: 2.406 W and 5.9 mm/s, bottom row: 0.965 W and 14.3 mm/s).

For 355 nm, all interaction regimes have a slope of roughly -1 on the $I - t_i$ diagram (Figure 8(a)), and because of that they appear nearly vertical on the corresponding $I - E'$ diagram (Figure 8(b)). This means that at this wavelength the amount of energy absorbed per unit length, rather than laser intensity, plays a critical role in determining the interaction regimes, so we can define interaction regimes in terms of several threshold energy values. On the other hand, for

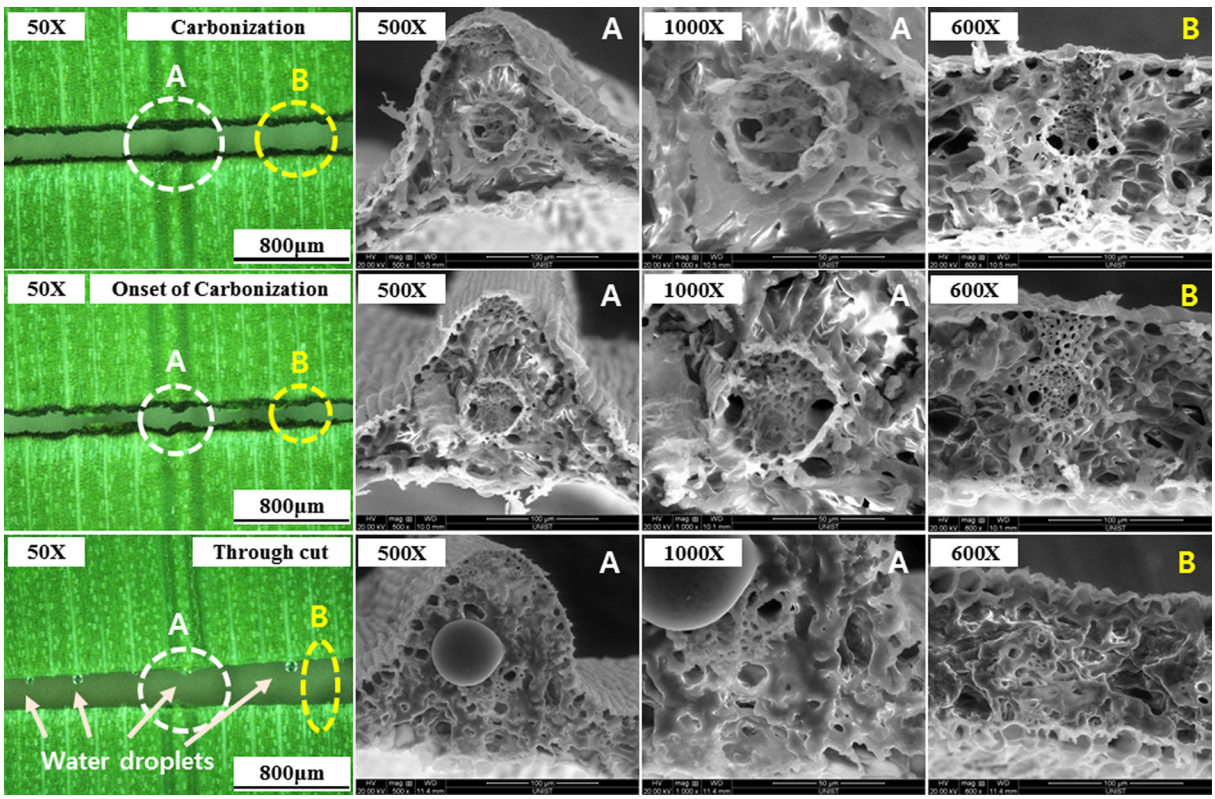

FIG. 7. Optical microscope and SEM images for 1064 nm (Top row: 13.8 W and 1 mm/s, middle row: 13.8 W and 2.4 mm/s, bottom row: 2.502 W and 5.9 mm/s).

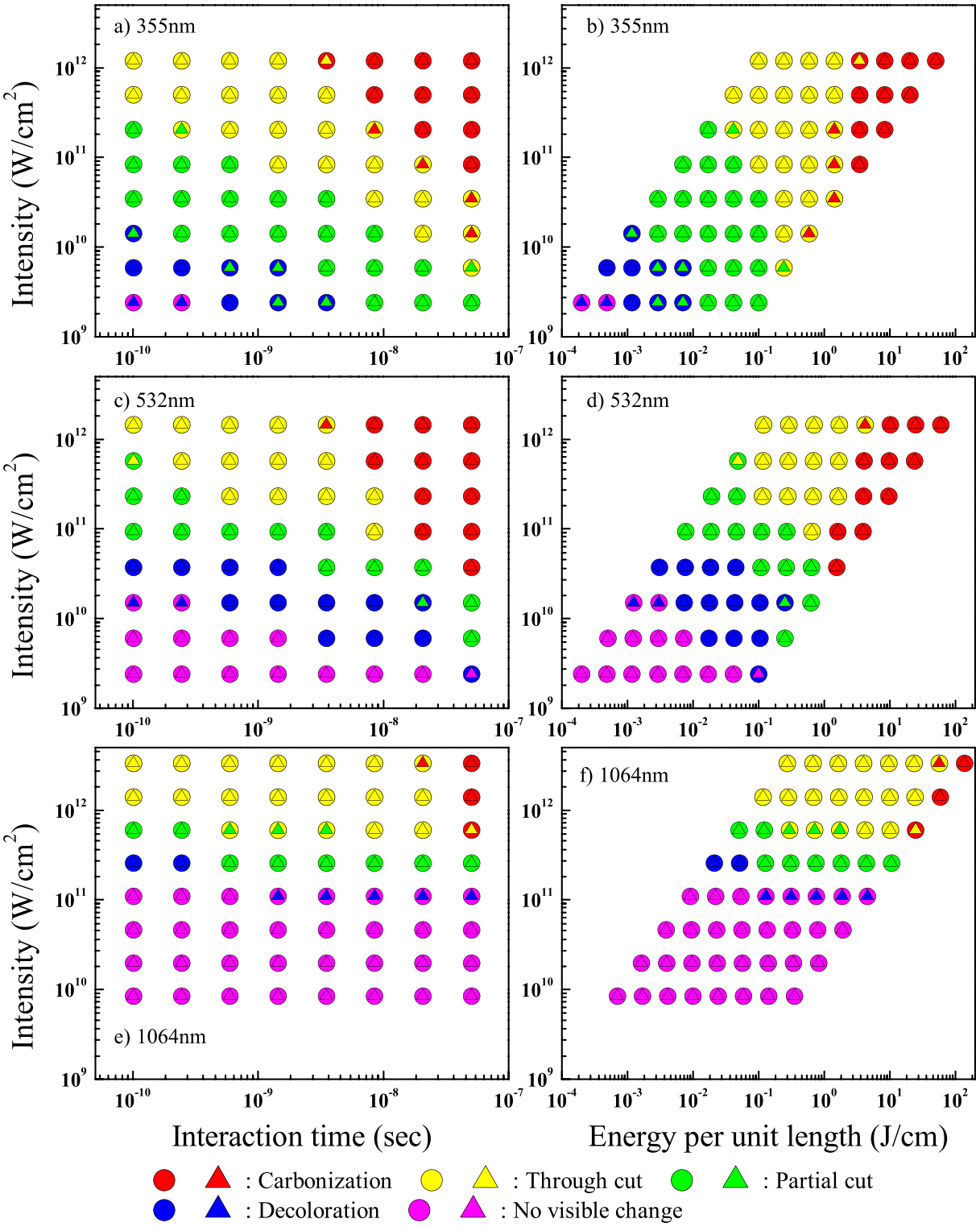

FIG. 8. Interaction maps for 355, 532, and 1064 nm constructed from experiments. For each wavelength, experiments were repeated twice. The results of the first and second data sets are shown as circles and triangles, respectively.

$\lambda = 1064$ nm, except for the carbonization regime, all the interaction regimes are virtually horizontal on both diagrams ((Figures 8(e) and 8(f)). In other words, in this case, the laser intensity, not the energy density, determines the interaction regimes. Although we are unable to find the exact causes of this difference, we believe that it is strongly related to the difference in light absorbing agents at these wavelengths. Recall that light is primarily absorbed by pigments at $\lambda = 355$ nm and by dry matter and water at $\lambda = 1064$ nm. In the case of 532 nm, interactions regimes, except for the carbonization regime, are neither vertical nor horizontal. Overall, the slope increases from no-visual-change to carbonization, which means that the process changes from intensity-driven to energy-driven.

Note that for all three wavelength cases, no-visual-change regions are largely horizontal although the experimental data for 355 nm is not enough due to the limitations in the experimental equipment. Therefore, we can say that the decoloration process is initiated at threshold intensity. This is reasonable because, decoloration seems to be caused by the damage in pigments as discussed earlier and pigments could be damaged when the light intensity is too high. For 1064 nm, the decoloration threshold is around 1.8×10^{11} W/cm^2 for a very wide range of interaction time ($42\,\mu s \sim 21$ ms) or scanning speed ($1 \sim 500$ mm/s). For 355 and 532 nm, the decoloration thresholds are roughly 2.4×10^9 W/cm^2 and 1.5×10^{10} W/cm^2, respectively. This wavelength-dependent threshold values for decoloration can be explained by the spectral absorption characteristics ($a \times C$) presented in Figure 2: the $a \times C$ value decreases as wavelength increases. The threshold intensity values for decoloration are summarized in Table V.

One more thing to note is that the carbonization regions are nearly vertical on the $I - E'$ diagram for all three wavelengths. We believe that carbonization is a chemical process that requires a certain amount of energy, so unlike the decoloration process it is less sensitive to laser intensity. As shown in Figure 8 (and also in Table V), carbonization threshold energy values for 355, 532, and 1064 nm are 1.4 J/cm, 2 J/cm, and 59 J/cm, respectively. As expected, the threshold energy increases as the wavelength increases.

In order to study these threshold energy values in more detail, we need to know the absorptance of grass at these wavelengths. Recently, Maiser calculated reflectance, transmittance, and absorptance for a number of plant leaves employing a Markov chain based method (*SLOPE*) with several concentration values of leaf constituents and leaf internal optical properties, such as scattering coefficient and back scattering ratio.[15] In Table VI, we summarized the ranges of R, T, and A for 355, 532, and 1064 nm that were obtained for banana leaves, linden leaves, and maple leaves. Among these, banana leaves are monocotyledonous like grass, and linden and maple leaves are dicotyledonous. Also, on the last column the absorptance values normalized by the absorptance at 1064 nm are presented. Although grass was not considered in his work, the simulation results show that reflectance (R), transmittance (T), and absorptance (A) do not change much for a wide range of leaf properties, so we will use his result as a guide for grass absorptance in this study.

As shown in Table VI, at 355 nm 96∼97% of the incident light energy is absorbed by typical plant leaves, and only 4∼7% of the light energy is absorbed when $\lambda = 1064$ nm. When $\lambda = 532$ nm, 76∼86% of the light energy is absorbed. Therefore, the ratio of energy absorbed for 355, 532, and 1064 nm is roughly 18:15:1. Meanwhile, the carbonization threshold energy ratio in Table V is 1:1.4:42 for 355, 532, and 1064 nm, respectively. Comparing the two ratios and considering that this is a simple qualitative analysis, we believe that this absorbed energy is indeed very closely related to the carbonization threshold energy.

One last thing to consider is the width of the combined regions consisting of decoloration, partial-cut, and through-cut regions, i.e., a region denoted by blue, green, and yellow colors altogether in Figure 8. For example, comparing Figures 8(a) and 8(c), the width is noticeably narrower for 532 nm. If we count the number of the corresponding data points in Figure 8, the band covers about 80% of the whole map for 355 nm and roughly 62.5% for 532 nm. We believe that this is because, as discussed above, decoloration and carbonization threshold values change differently as the wavelength changes.

TABLE V. Threshold values for decoloration and carbonization (from Figure 8).

λ (nm)	Decoloration (W/cm^2)	Carbonization (J/cm)
355	$\sim 2.4 \times 10^9$	~ 1.4
532	$\sim 1.5 \times 10^{10}$	~ 2
1064	$\sim 1.8 \times 10^{11}$	~ 59

TABLE VI. Calculated leaf reflectance, transmittance, and absorptance data averaged for banana leaves, linden leaves, and maple leaves.[15]

λ (nm)	R	T	A	A/A_{1064}
355	0.03∼0.04	∼0	0.96∼0.97	18
532	0.06∼0.11	0.08∼0.15	0.76∼0.86	15
1064	0.42∼0.50	0.46∼0.54	0.04∼0.07	1

V. CONCLUSION

In this article, we have studied laser interaction with grass tissues using 355, 532, and 1064 nm picosecond lasers. Although picosecond lasers were used, the experimental results indicated that the interactions could be thermal and carbonization occurred at high laser energy density. In this study, grass was selected, but we believe the results can be at least qualitatively applied to other green plant leaves because the optical properties of leaves are governed by pigments, water, and dry matter in leaves. After identifying five interaction regimes, we have constructed an interaction map for each wavelength, which we believe is useful in understanding how grass interacts with lasers. In this study, we have found that for the decoloration process threshold intensity exists and, on the contrary, threshold energy is a more suitable concept to explain carbonization.

ACKNOWLEDGMENTS

This research was supported by the Basic Science Research Program through the National Research Foundation (NRF) of Korea funded by the Ministry of Education, Science and Technology (Grant No. 2010-0005744).

[1]M. H. Niemz, *Laser-Tissue Interactions: Fundamentals and Applications*, 3rd, enlarged ed. (Springer-Verlag, Berlin, Germany, 2004).
[2]J. Kolar, M. Strlic, S. Pentzien, and W. Kautek, "Near-UV, visible and IR pulsed laser light interaction with cellulose," Appl. Phys. A **71**, 87–90 (2000).
[3]M. Oujja, E. Rebollar, C. Abrusci, A. Del Amo, F. Catalina, and M. Castillejo, "UV, visible and IR laser interaction with gelatine," in COLA'05: 8th International Conference on Laser Ablation (Banff, Canada, 2007), Vol. 59, pp. 571–574.

[4]J. Kolar, M. Strlic, D. Muller-Hess, A. Gruber, K. Troschke, S. Pentzien, and W. Kautek, "Near-UV and visible pulsed laser interaction with paper," J. Cultural Heritage **1**, S221–S224 (2000).
[5]H. Ki, "On vaporization in laser material interaction," J. Appl. Phys. **107**, 104908 (2010).
[6]H. Y. Li and H. S. Ki, "Effect of ionization on femtosecond laser pulse interaction with silicon," J. Appl. Phys. **100**, 104907 (2006).
[7]D. J. Lim, H. Ki, and J. Mazumder, "Mass removal modes in the laser ablation of silicon by a Q-switched diode-pumped solid-state laser (DPSSL)," J. Phys. D **39**, 2624–2635 (2006).
[8]R. Ortiz, I. Quintana, J. Etxarri, A. Lejardi, and J. R. Sarasua, "Picosecond laser ablation of poly-L-lactide: Effect of crystallinity on the material response," J. Appl. Phys. **110**, 094902 (2011).
[9]D. Marla, U. V. Bhandarkar, and S. S. Joshi, "Critical assessment of the issues in the modeling of ablation and plasma expansion processes in the pulsed laser deposition of metals," J. Appl. Phys. **109**, 021101 (2011).
[10]S. Heiroth, J. Koch, T. Lippert, A. Wokaun, D. Gunther, F. Garrelie, and M. Guillermin, "Laser ablation characteristics of yttria-doped zirconia in the nanosecond and femtosecond regimes," J. Appl. Phys. **107**, 014908 (2010).
[11]H.-W. Heldt and B. Piechulla, *Plant Biochemistry*, 4th ed. (Academic, 2010).
[12]See http://en.wikipedia.org/wiki/Lawn#North_America for Lawn.
[13]J. B. Feret, C. Francois, G. P. Asner, A. A. Gitelson, R. E. Martin, L. P. R. Bidel, S. L. Ustin, G. le Maire, and S. Jacquemoud, "PROSPECT-4 and 5: Advances in the leaf optical properties model separating photosynthetic pigments," Remote Sens. Environ. **112**, 3030–3043 (2008).
[14]G. M. Hale and M. R. Querry, "Optical-constants of water in 200-Nm to 200-Mum wavelength region," Appl. Opt. **12**, 555–563 (1973).
[15]S. W. Maiser, "Modeling the radiative transfer in leaves in the 300nm to 2.5um wavelength region taking into consideration chlorophyll fluorescence— the leaf model SLOPE," Ph.D. dissertation, Technische University Munchen, Germany, 2000.
[16]S. Jacquemoud and F. Baret, "PROSPECT: A model of leaf optical-properties spectra," Remote Sens. Environ. **34**, 75–91 (1990).
[17]S. Jacquemoud, S. L. Ustin, J. Verdebout, G. Schmuck, G. Andreoli, and B. Hosgood, "Estimating leaf biochemistry using the PROSPECT leaf optical properties model," Remote Sens. Environ. **56**, 194–202 (1996).
[18]X. Dong, B. Patton, P. Nyren, R. Limb, L. Cihacek, D. Kirby, and E. Deckard, "Leaf-water relations of a native and an introduced grass species in the mixed-grass prairie under cattle grazing," Appl. Ecol. Environ. Res. **9**, 311–331 (2011).
[19]M. G. Lefsrud, J. C. Sorochan, D. A. Kopsell, and J. S. McElroy, "Pigment Concentrations among Heat-tolerant Turfgrasses," Hortscience **45**, 650–653 (2010).